Cell Reports, Volume *22*

Supplemental Information

Reciprocal TCR-CD3 and CD4 Engagement of a Nucleating pMHCII Stabilizes a Functional Receptor Macrocomplex

Caleb R. Glassman, Heather L. Parrish, Mark S. Lee, and Michael S. Kuhns

SUPPLEMENTAL EXPERIMENTAL PROCEDURES

Cell lines and constructs

58$\alpha^-\beta^-$ and M12 cells were generated by retroviral transduction using the MSCV-based retroviral expression vectors pP2 (IRES-puromycin resistance) and pZ4 (IRES-zeocin resistance) (Glassman et al., 2016; Lee et al., 2015; Parrish et al., 2016).

Proteins encoded by the constructs used in this study are described by amino acid (aa) number beginning at the start methionine (UniProt convention). Constructs encoding cDNA for the B3K506 and B3K508 TCRs were kindly provided by Eric Huseby and used for PCR amplification for cloning into pP2 (TCRβ) and pZ4 (TCRα). The 5c.c7 or 2B4 TCR, which are specific for moth cytochrome c (88-103) presented in I-E^k, or the B3K506 or B3K508 TCRs specific for the 3K peptide presented in I-A^b were expressed with full length or C-terminally truncated CD3 subunits (CD3δT aa:1-132, CD3γT aa:1-143, CD3εT aa:1-139, and CD3ζT aa:1-57) along with a C-terminally truncated CD4 (CD4T aa:1-421)(Glassman et al., 2016). CD4T variants used in this study were $CD4T^{\Delta bind}$ (aa: 68-73 KGVLIR to DGDSDS), $CD4T^{P228E+F231E}$ and $CD4T^{P281E}$.

For 58$\alpha^-\beta^-$ lines, the C-terminus of the 5c.c7 α chain, 2B4 β chain, B3K506 β chain or B3K508 β chain was fused to mEGFP via a long flexible linker (AAAGGGGSGGGGSGGGGS), the 5c.c7 β chain, 2B4 α chain, B3K506 α chain, B3K508 α chain and CD4T were encoded by independent constructs and full-length CD3 subunits were encoded by a poly-cistronic construct as previously described (Glassman et al., 2016; Parrish et al., 2016).

5c.c7$^+$ M12 lines were generated using constructs encoding CD3εT-T2A-5c.c7α, CD3ζT-T2A-5c.c7β, $CD3\delta T^G$-T2A-CD3γT and $CD4T^{mCh}$. CD3δT was fused to mEGFP via a flexible GGSAAG linker and CD4 was fused to mCherry via an AAAG linker as previously described (Glassman et al., 2016). CD3ζT was fused via a GGSAAG linker to the biotin acceptor peptide, AP-3, a short tag that was considered irrelevant for the current study. 2B4$^+$ M12 lines were generated using constructs encoding 2B4α, $2B4\beta^G$, $CD4T^{mCh}$, and a polycystronic construct encoding C-terminally truncated CD3 subunits. The 2B4 β chain was fused to mEGFP via a long flexible linker (AAAGGGGSGGGGSGGGGS) and CD4 was fused to mCherry via an AAAG linker as previously described (Glassman et al., 2016).

APCs were generated by transducing M12 or 58$\alpha^-\beta^-$ cells with full-length I-$E^k\alpha$ or I-$A^b\alpha$ and full-length I-$E^k\beta$ or I-$A^b\beta$ fused via the N-terminus to a peptide as previously described (Parrish et al., 2016; Parrish et al., 2015). Peptides bound to I-E^k in this study were moth cytochrome c (MCC 88-103), the altered peptide ligands T102S and

T102G, and the mouse hemoglobin d allele (Hb 64-76). Peptides bound to I-A^b in this study were Ova 326-338, 3K and the altered peptide ligands P-1A and P5R (Huseby et al., 2006).

Cell surface expression of CD4 (mAb clone GK1.5 e450 eBioscience), TCRα (Vα11, mAb clone RR8-1 allophycocyanin eBioscience), TCRβ (Vβ3, mAb clone KJ25 PE BD Biosciences), I-E^k (mAb clone 14-4-4S) and I-A^b (mAb clone KH74) were determined by flow cytometry as indicated in the figures. The P281E mutation reduced cell surface expression on 58$\alpha^-\beta^-$ cells, so lines were FACS sorted using a non-blocking CD4 antibody (mAb clone RM4-4 PE Biolegend).

Functional assays

For peptide titration experiments, 5 X 10^4 5c.c7 TCR transgenic spleenocytes or thymocytes or 5 X 10^4 58$\alpha^-\beta^-$ cells were co-cultured with 1 X 10^5 M12 I-E^k cells and MCC 88-103, T102S, or T102G peptide at the indicated concentration in 96-well round-bottom plates and peptides were purchased at ninety percent purity from 21st Century Biochemicals, Inc. In indicated experiments, anti-CD4 (mAb clone GK1.5) or anti-CD8 (control, mAb clone 53.6-7) was added at 20μg/mL. Supernatants were harvested for IL-2 ELISA after 16 hours co-culture as described below. Thymocyte co-cultures were incubated for 14 hours at 37°C and stained for Vα11 (mAb clone RR8-1, APC, eBiosciences), CD8β (mAb clone YTS156.7.7, PerCpCy5.5, Biolegend), CD4 (mAb clone Rm4-4, Pacific Blue, Biolegend), CD69 (mAb clone H1-2F3, PE, eBiosciences) and AnnexinV (FITC, Biolegend). For tethered peptide co-cultures, 5 X 10^4 58$\alpha^-\beta^-$ cells were cultured with 1 X 10^5 M12 cells expressing I-E^k tethered to MCC, T102S, T102G or Hb in 96-well round-bottom plates. IL-2 was normalized to the CD4T control for each set of cell lines within each condition to allow for comparison between multiple independently generated cell lines. IL-2 was quantified by ELISA from supernatants after 16 hours co-culture at 37°C for all experiments. Anti-mouse IL-2 (clone JES6-1A12, Biolegend) was used as a capture antibody and biotin anti-mouse IL-2 (clone JES6-5H4, Biolegend) was used as the secondary antibody. Streptavidin-HRP and TMB substrate (Biolegend) were used for detection.

TCR downregulation and CD69 upregulation were measured on T cell hybridomas following 16 hours of co-culture with M12 cells. Cells were pipetted to break apart M12:58$\alpha^-\beta^-$ cell couples, incubated in mAb clone 2.4G2 supernatant to block Fc receptors, and then stained with anti-CD4 (clone GK1.5, e450), CD69 (clone H1.2F3, PE) and Vα11 (clone RR8-1, APC) mAbs. CD69 or Vα11 gMFI was determined for GFP positive and CD4

expression matched 58$\alpha^-\beta^-$ cells and normalized to the gMFI of cells cultured with the Hb:I-E^k controls for each cell line.

Cell coupling

TCR^+ cells expressing mEGFP were combined with Tag-It Violet (Biolegend) loaded APCs expressing tethered pMHCII at a 1:1 ratio. Cells were incubated for 1 hour at 37°C and analyzed by flow cytometry (Egen and Allison, 2002). Couple formation was assessed as the ratio of GFP (TCR^+) Violet ($pMHCII^+$) double positive events divided by the total number of GFP positive events. This was then normalized to CD4T cells interacting with MCC:I-E^k or 3K:I-A^b expressing APCs to allow comparison between multiple experiments. In some experiments, kinase activity was blocked by incubating cells with 20μM PP2 (Calbiochem) or DMSO vehicle control (0.2%) for 20 minutes at 37°C prior to cell coupling.

Soluble proteins for bilayers and immobile surfaces

ICAM-1 and pMHCII production were described previously (Glassman et al., 2016).

Lipid bilayers

Unilaminar vesicles were generated by extruding a lipid mixture consisting of 97.5mol % POPC, 1 mol % DGS NiNTA, 1 mol biotin-CAP PE and 0.5 mol % DOPE-PEG5000 (Avanti Polar Lipids) (Glassman et al., 2016). Bilayers were formed on cleaned glass coverslips and functionalized with 0.05 μg/well MCC:I-E^k and 0.08μg/well ICAM-1 to give a pMHCII density of ~60molecules/μm^2.

Immobile surfaces

Biotinylated poly-L-lysine coated coverslips were coated with 5μg/mL streptavidin, washed and incubated with 5μg/mL pMHCII biotin plus 0.5μg/mL biotinylated anti H2-D^d, which was used to ensure cell attachment (Glassman et al., 2016; Huse et al., 2007).

Microscopy

Total internal reflection fluorescence microscopy (TIRFM) was performed as previously described (Glassman et al., 2016). In brief, cells were allowed to interact with the imaging surface for 20' prior and then imaged for 20-30'.

Data were collected with a Marianas workstation built on a Zeiss Axio Observer Z1 (Intelligent Imaging Innovations, 3I) using a 63x Zeiss TIRF objective coupled to a Zeiss motorized TIRF slider (numerical aperture 1.46). Illumination was achieved with a Laser Stack (3I) containing 50mW 488nm and 561 solid-state lasers at 20% output. Photoablation was performed using a Vector high-speed point scanner (3I) at 100% laser power within a 6.45μm^2 region of interest (ROI) and images were collected using a Photometrics Evolve EMCCD camera (1 pixel= 0.25μm (H) x 0.25μm (V)). Receptor accumulation images consisted of TIRF and brightfield images collected at a single time point. For Fluorescence Recovery After Photobleaching (FRAP) acquisitions, fluorescence images were acquired at 3 sec intervals. Donor Recovery after Acceptor Photobleaching images were acquired at 500ms intervals.

$FRET_E$ analysis

Donor Recovery after Acceptor Photobleaching was performed as previously described (Glassman et al., 2016). Analyzed cells had bleaching below 12.5% of prebleach mCherry intensity. Subsets were matched for mCherry intensity, mEGFP intensity (postbleach) and mEGFP/mCherry ratio in TIRF. FRET efficiency ($FRET_E$) was calculated using: $FRET_E = 1 - Q/DQ$ where Q is the mEGFP intensity prior to photobleaching and DQ is the mEGFP intensity following mCherry ablation.

SUPPLEMTAL REFERENCES

Aivazian, D., and Stern, L.J. (2000). Phosphorylation of T cell receptor zeta is regulated by a lipid dependent folding transition. Nat Struct Biol *7*, 1023-1026.

Egen, J.G., and Allison, J.P. (2002). Cytotoxic T lymphocyte antigen-4 accumulation in the immunological synapse is regulated by TCR signal strength. Immunity *16*, 23-35.

Glassman, C.R., Parrish, H.L., Deshpande, N.R., and Kuhns, M.S. (2016). The CD4 and CD3deltaepsilon Cytosolic Juxtamembrane Regions Are Proximal within a Compact TCR-CD3-pMHC-CD4 Macrocomplex. J Immunol *196*, 4713-4722.

Huppa, J.B., Axmann, M., Mortelmaier, M.A., Lillemeier, B.F., Newell, E.W., Brameshuber, M., Klein, L.O., Schutz, G.J., and Davis, M.M. (2010). TCR-peptide-MHC interactions in situ show accelerated kinetics and increased affinity. Nature *463*, 963-967.

Huse, M., Klein, L.O., Girvin, A.T., Faraj, J.M., Li, Q.J., Kuhns, M.S., and Davis, M.M. (2007). Spatial and temporal dynamics of T cell receptor signaling with a photoactivatable agonist. Immunity *27*, 76-88.

Huseby, E.S., Crawford, F., White, J., Marrack, P., and Kappler, J.W. (2006). Interface-disrupting amino acids establish specificity between T cell receptors and complexes of major histocompatibility complex and peptide. Nat Immunol *7*, 1191-1199.

Jonsson, P., Southcombe, J.H., Santos, A.M., Huo, J., Fernandes, R.A., McColl, J., Lever, M., Evans, E.J., Hudson, A., Chang, V.T.*, et al.* (2016). Remarkably low affinity of CD4/peptide-major histocompatibility complex class II protein interactions. Proc Natl Acad Sci U S A *113*, 5682-5687.

Kuhns, M.S., and Badgandi, H.B. (2012). Piecing together the family portrait of TCR-CD3 complexes. Immunol Rev *250*, 120-143.

Lee, M.S., Glassman, C.R., Deshpande, N.R., Badgandi, H.B., Parrish, H.L., Uttamapinant, C., Stawski, P.S., Ting, A.Y., and Kuhns, M.S. (2015). A Mechanical Switch Couples T Cell Receptor Triggering to the Cytoplasmic Juxtamembrane Regions of CD3zetazeta. Immunity *43*, 227-239.

Nika, K., Soldani, C., Salek, M., Paster, W., Gray, A., Etzensperger, R., Fugger, L., Polzella, P., Cerundolo, V., Dushek, O.*, et al.* (2010). Constitutively active Lck kinase in T cells drives antigen receptor signal transduction. Immunity *32*, 766-777.

Parrish, H.L., Deshpande, N.R., Vasic, J., and Kuhns, M.S. (2016). Functional evidence for TCR-intrinsic specificity for MHCII. Proc Natl Acad Sci U S A.

Parrish, H.L., Glassman, C.R., Keenen, M.M., Deshpande, N.R., Bronnimann, M.P., and Kuhns, M.S. (2015). A Transmembrane Domain GGxxG Motif in CD4 Contributes to Its Lck-Independent Function but Does Not Mediate CD4 Dimerization. PLoS One *10*, e0132333.

Shi, X., Bi, Y., Yang, W., Guo, X., Jiang, Y., Wan, C., Li, L., Bai, Y., Guo, J., Wang, Y.*, et al.* (2013). Ca2+ regulates T-cell receptor activation by modulating the charge property of lipids. Nature *493*, 111-115.

Vignali, D.A., and Vignali, K.M. (1999). Profound enhancement of T cell activation mediated by the interaction between the TCR and the D3 domain of CD4. J Immunol *162*, 1431-1439.

Wang, J.H., Meijers, R., Xiong, Y., Liu, J.H., Sakihama, T., Zhang, R., Joachimiak, A., and Reinherz, E.L. (2001). Crystal structure of the human CD4 N-terminal two-domain fragment complexed to a class II MHC molecule. Proc Natl Acad Sci U S A *98*, 10799-10804.

Xu, C., Gagnon, E., Call, M.E., Schnell, J.R., Schwieters, C.D., Carman, C.V., Chou, J.J., and Wucherpfennig, K.W. (2008). Regulation of T cell receptor activation by dynamic membrane binding of the CD3epsilon cytoplasmic tyrosine-based motif. Cell *135*, 702-713.

Yin, Y., Wang, X.X., and Mariuzza, R.A. (2012). Crystal structure of a complete ternary complex of T-cell receptor, peptide-MHC, and CD4. Proceedings of the National Academy of Sciences of the United States of America *109*, 5405-5410.

Zhang, H., Cordoba, S.P., Dushek, O., and Anton van der Merwe, P. (2011). Basic residues in the T-cell receptor zeta cytoplasmic domain mediate membrane association and modulate signaling. Proceedings of the National Academy of Sciences of the United States of America *108*, 19323-19328.

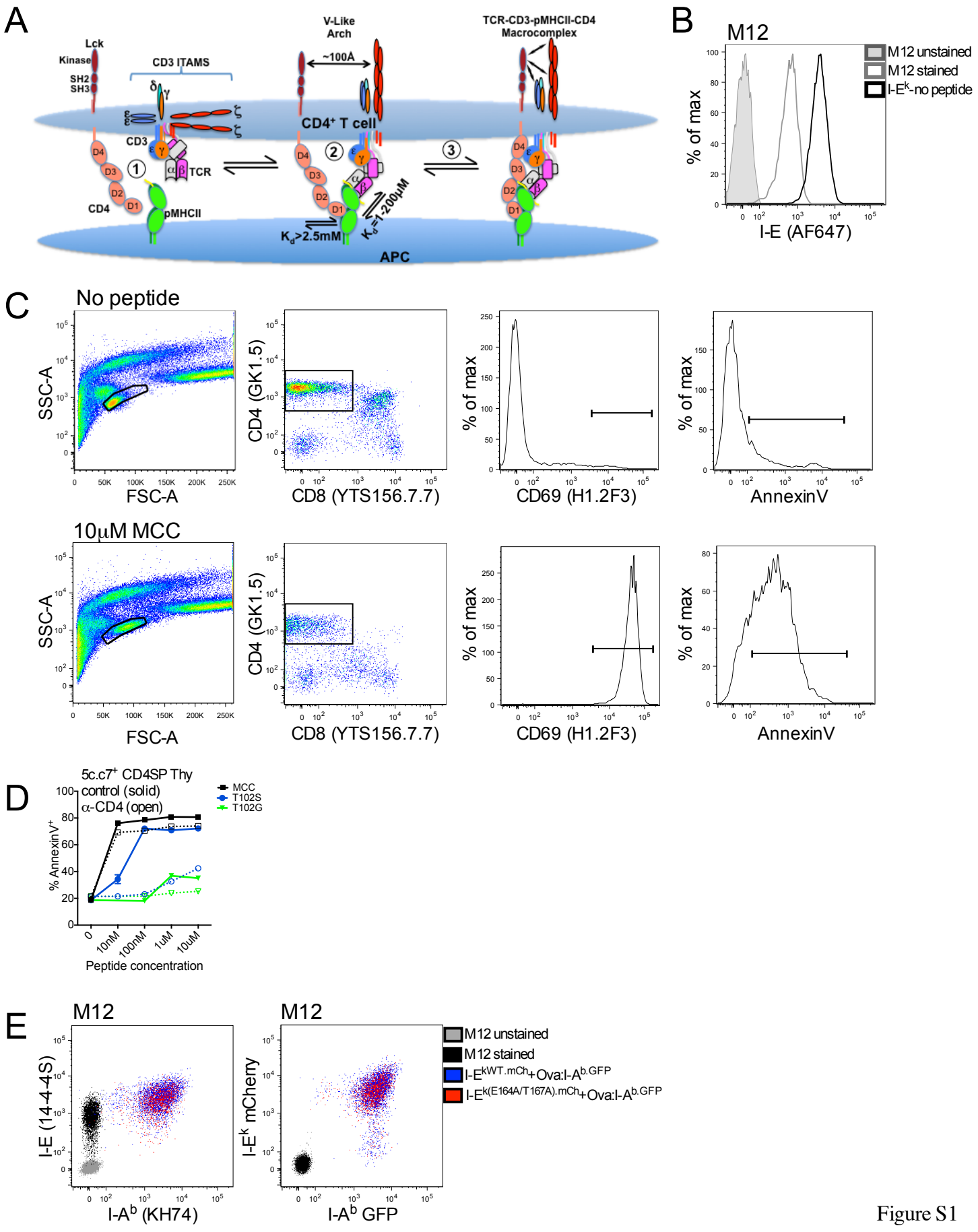
A
Lck
Kinase
SH2
SH3
CD3 ITAMS
V-Like
Arch
~100Å
TCR-CD3-pMHCII-CD4
Macrocomplex
CD4+ T cell
CD3
TCR
CD4
pMHCII
APC
K_d>2.5mM
K_d=1-200μM
B
M12
M12 unstained
M12 stained
I-E^k-no peptide
% of max
I-E (AF647)
C
No peptide
10μM MCC
SSC-A
FSC-A
CD4 (GK1.5)
CD8 (YTS156.7.7)
% of max
CD69 (H1.2F3)
AnnexinV
D
5c.c7$^+$ CD4SP Thy
control (solid)
α-CD4 (open)
MCC
T102S
T102G
% AnnexinV$^+$
Peptide concentration
0
10nM
100nM
1uM
10uM
E
M12
M12
I-E (14-4-4S)
I-A^b (KH74)
I-E^k mCherry
I-A^b GFP
M12 unstained
M12 stained
I-E$^{kWT.mCh}$+Ova:I-A$^{b.GFP}$
I-E$^{k(E164A/T167A).mCh}$+Ova:I-A$^{b.GFP}$

Figure S1

Figure S1. Models and cellular characterization, related to Figure 1.
(**A**) Graphical model depicting the possible assembly of a TCR-CD3-pMHCII-CD4 macrocomplex. (**1**) The unengaged TCR-CD3 complex is shown with CD3ε and CD3ζζ ITAMs associated with the inner leaf of the T cell membrane (Aivazian and Stern, 2000; Shi et al., 2013; Xu et al., 2008). CD4 is shown associated with an active Lck on a T cell surface (upper blue sphere)(Nika et al., 2010). The surface of an APC (lower blue sphere) is shown with a pMHCII. (**2**) The V-like arch model is shown as possible intermediate in the formation of a compact macrocomplex (Wang et al., 2001; Yin et al., 2012). The solution K_d are noted for CD4-MHCII and agonist to weak agonist TCR-pMHCII interactions (Huppa et al., 2010; Jonsson et al., 2016). the ITAMs are shown free of the membrane based on previous studies (Shi et al., 2013; Xu et al., 2008; Zhang et al., 2011). (**3**) The final subunit assembly of a compact TCR-CD3-pMHCII-CD4 macrocomplex (Kuhns and Badgandi, 2012). The low affinity of CD4-MHCII interactions in the D1 domain would allow CD4 to dock along the composite surface of the TCR-CD3-pMHCII axis created by TCR-pMHCII interactions. This is proposed to position Lck in the proper spatial relationship with the ITAMs for the appropriate duration to initiate signaling.
(**B**) Surface expression of I-E^k on M12 I-E^{k+} cells.
(**C**) Gating scheme for CD69 and AnnexinV levels on $CD4^+$ 5c.c7 TCR tg thymocytes. Total thymocytes were cultured with I-E^{k+} M12 cells and a titration of the indicated peptides for 14 hours prior to analysis.
(**D**) Percent of $CD4^+$ 5c.c7 TCR tg thymocytes that were $AnnexinV^+$. Data from C and D are representative of three experiments.
(**E**) Expression of I-E^k and I-A^b on M12 cells expressing I-$E^{k.WT.mCh}$ or I-$E^{k.E164A/T167A.mCh}$ and I-$A^{b.GFP}$-Ova.

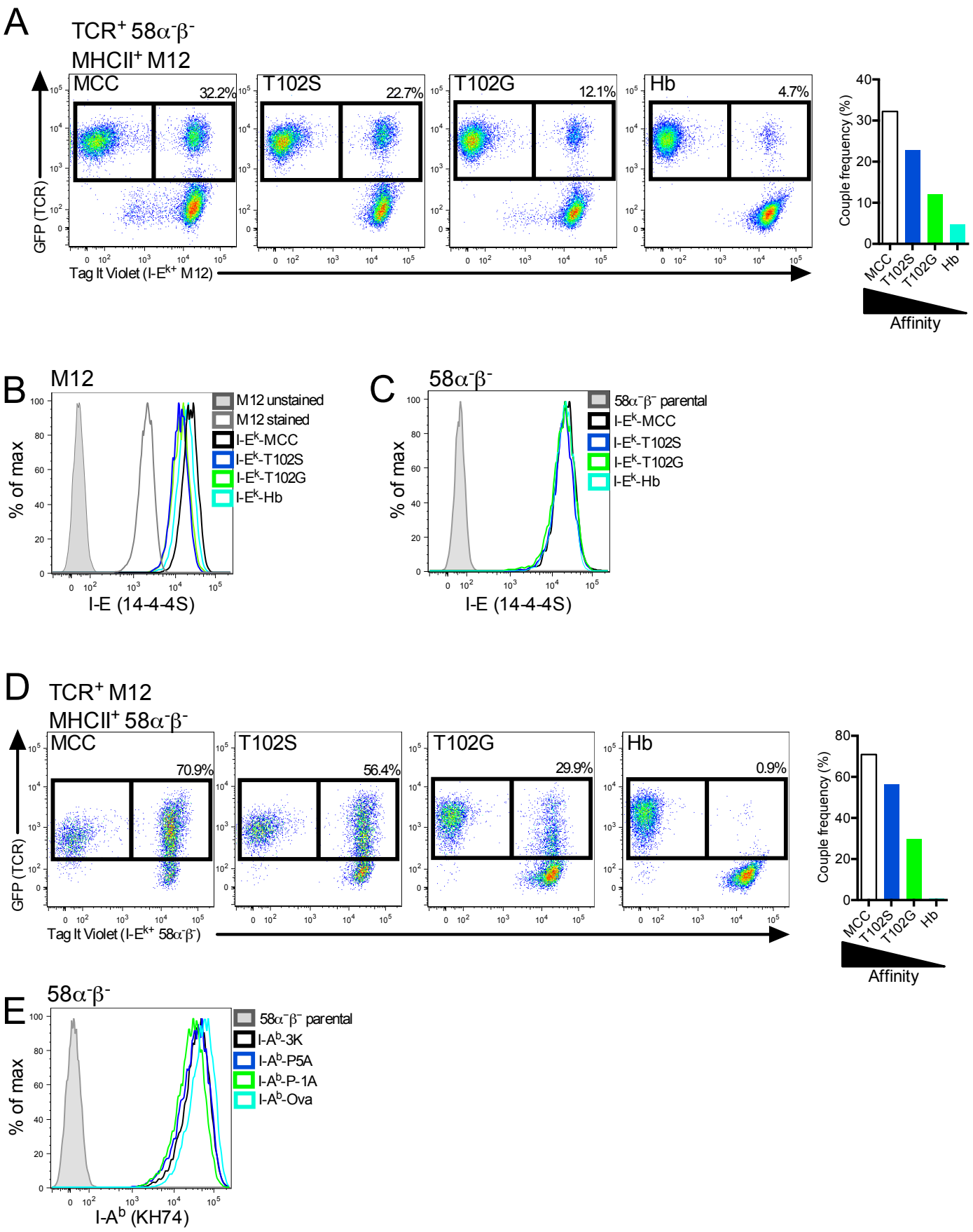
A
TCR+ 58α-β-
MHCII+ M12
MCC
32.2%
T102S
22.7%
T102G
12.1%
Hb
4.7%
GFP (TCR)
Tag It Violet (I-Ek+ M12)
Couple frequency (%)
MCC
T102S
T102G
Hb
Affinity
B
M12
% of max
M12 unstained
M12 stained
I-Ek-MCC
I-Ek-T102S
I-Ek-T102G
I-Ek-Hb
I-E (14-4-4S)
C
58α-β-
58α-β- parental
I-Ek-MCC
I-Ek-T102S
I-Ek-T102G
I-Ek-Hb
I-E (14-4-4S)
D
TCR+ M12
MHCII+ 58α-β-
MCC
70.9%
T102S
56.4%
T102G
29.9%
Hb
0.9%
GFP (TCR)
Tag It Violet (I-Ek+ 58α-β-)
Couple frequency (%)
MCC
T102S
T102G
Hb
Affinity
E
58α-β-
% of max
58α-β- parental
I-Ab-3K
I-Ab-P5A
I-Ab-P-1A
I-Ab-Ova
I-Ab (KH74)

Figure S2

Figure S2. Cell-cell coupling, related to Figure 2.

(**A**) Representative dot plots and quantification of 5c.c7^{+} 58$\alpha^{-}\beta^{-}$ cells expressing TCRα^{G} incubated with M12 cells expressing the indicated tethered pMHCII. Data are representative of three experiments.

(**B-C**) Expression of tethered-pMHCII on I-E^{k+} (**B**) M12 or (**C**) 58$\alpha^{-}\beta^{-}$ cells.

(**D**) Representative dot plots and quantification of 5c.c7^{+} M12 cells expressing CD3T subunits with CD3δT^{G} and CD4T incubated with 58$\alpha^{-}\beta^{-}$ cells expressing I-E^{k} and the indicated tethered peptide. Data are representative of three experiments.

(**E**) Expression of tethered-pMHCII on I-A^{b+} 58$\alpha^{-}\beta^{-}$ cells.

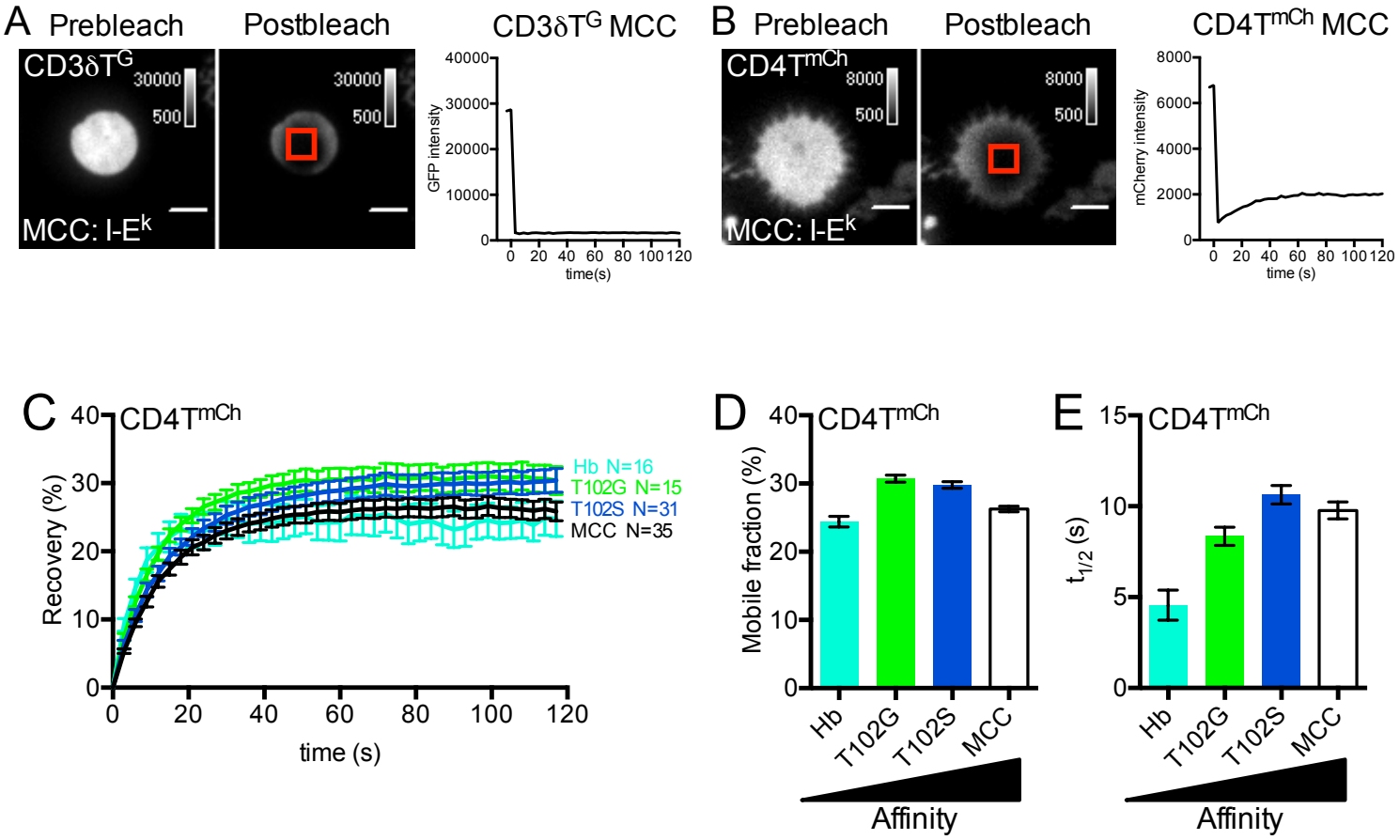
A
Prebleach
Postbleach
CD3δT^G MCC
CD3δT^G
30000
500
MCC: I-E^k
GFP intensity
time(s)
B
Prebleach
Postbleach
CD4T^mCh MCC
CD4T^mCh
8000
500
MCC: I-E^k
mCherry intensity
time (s)
C
CD4T^mCh
Recovery (%)
time (s)
Hb N=16
T102G N=15
T102S N=31
MCC N=35
D
CD4T^mCh
Mobile fraction (%)
Hb
T102G
T102S
MCC
Affinity
E
CD4T^mCh
t1/2 (s)
Hb
T102G
T102S
MCC
Affinity

Figure S3

Figure S3. Fluorescence recovery after photobleaching, related to Figure 3.
(**A-B**) Representative images and quantification of FRAP. 5c.c7^{+} M12 cells expressing CD3T subunits with CD3δT^{G} and CD4T^{mCh} were adhered to immobile surfaces presenting MCC:I-E^{k} for 20' prior to acquisition. Background subtracted TIRF images of (**A**) CD3δT^{G} and (**B**) CD4T^{mCh} before and after photobleaching with 488 and 561nm laser light, respectively. Traces show quantification of red-boxed region of interest (ROI) for 2 min at 3 second intervals following photobleaching. Scale bars represent 5μm and look up tables indicate fluorescence intensity of the photobleached channel.
(**C-H**) FRAP analysis of 2B4^{+} M12 cells expressing truncated CD3 subunits and CD4T^{mCh}. Cells were adhered to I-E^{k} coated surfaces presenting the indicated peptide. (**C**) Recovery traces for mCherry represent mean ± SEM for the indicated number of cells. (**D**) Mobile fraction (%) and (**E**) half-life ($t_{1/2}$) for recovery were determined by curve fitting. Error bars indicate 95% confidence interval.

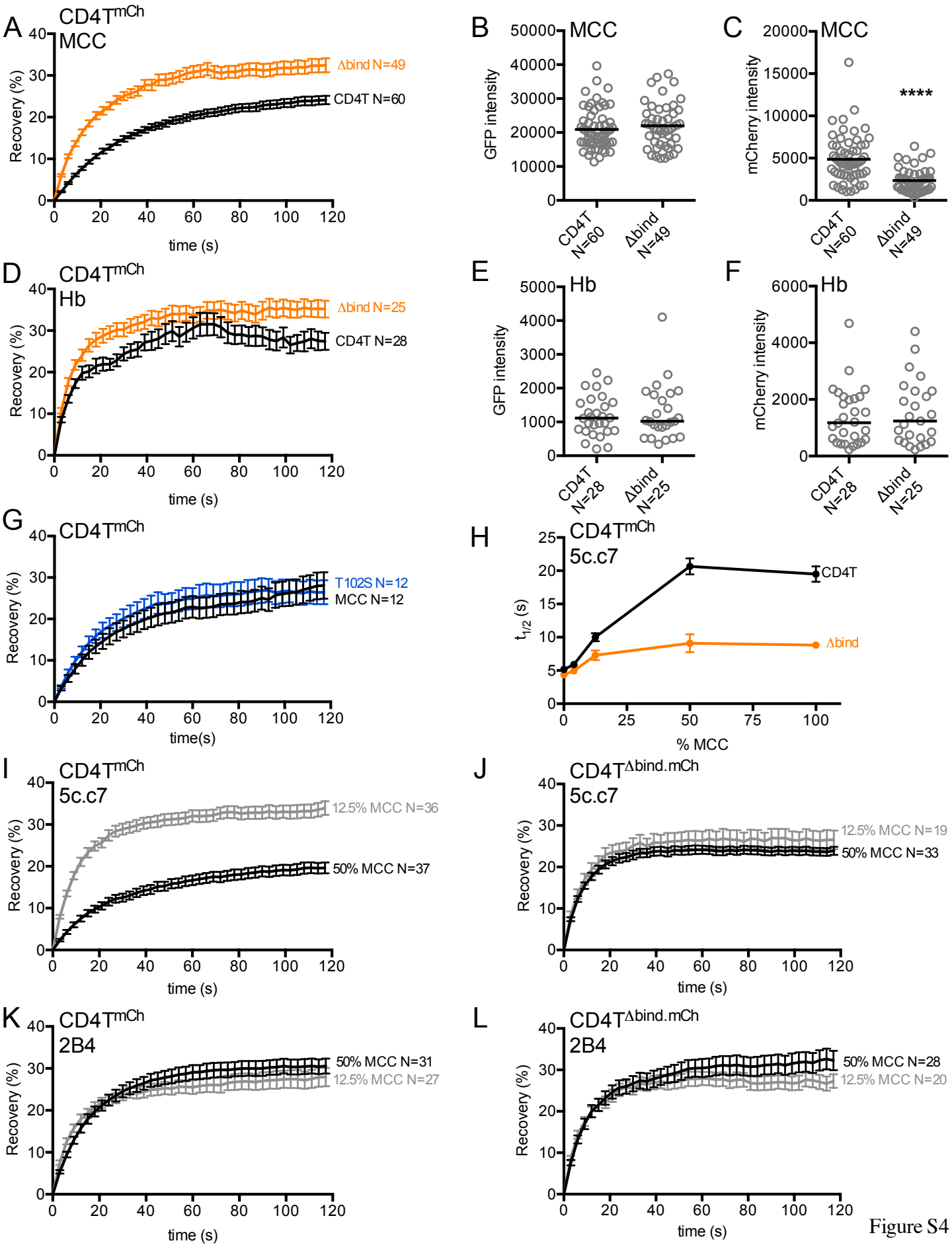
A
CD4T^mCh
MCC
Recovery (%)
time (s)
Δbind N=49
CD4T N=60
B
MCC
GFP intensity
CD4T N=60
Δbind N=49
C
MCC
mCherry intensity
****
CD4T N=60
Δbind N=49
D
CD4T^mCh
Hb
Recovery (%)
time (s)
Δbind N=25
CD4T N=28
E
Hb
GFP intensity
CD4T N=28
Δbind N=25
F
Hb
mCherry intensity
CD4T N=28
Δbind N=25
G
CD4T^mCh
Recovery (%)
time(s)
T102S N=12
MCC N=12
H
CD4T^mCh
5c.c7
t1/2 (s)
% MCC
CD4T
Δbind
I
CD4T^mCh
5c.c7
Recovery (%)
time (s)
12.5% MCC N=36
50% MCC N=37
J
CD4T^Δbind.mCh
5c.c7
Recovery (%)
time (s)
12.5% MCC N=19
50% MCC N=33
K
CD4T^mCh
2B4
Recovery (%)
time (s)
50% MCC N=31
12.5% MCC N=27
L
CD4T^Δbind.mCh
2B4
Recovery (%)
time (s)
50% MCC N=28
12.5% MCC N=20

Figure S4

Figure S4. CD4 recovery, related to Figure 4.
(A-F) CD4 recovery of 5c.c7^{+} M12 cells expressing truncated CD3 subunits with CD3δT^{G} and CD4T^{mCh} or CD4T$^{\Delta bind.\ mCh}$. Cells were adhered to immobile surfaces coated with MCC:I-E^{k} (**A-C**) or Hb:I-E^{k} (**D-F**). Panels on the left show recovery of CD4T^{mCh}. Right-hand panels show mCh intensity prebleach and GFP intensity postbleach. Data correspond to bar graphs in Figure 4A-D.
(**G**) CD4T recovery of pairwise matched 5c.c7^{+} M12 cells as shown in Figure 4E-H.
(**H-L**) CD4T recovery in response to varying doses of MCC:I-E^{k}. 5c.c7^{+} (**H,I,J**) or 2B4^{+} (**K,L**) M12 cells were adhered to immobile surfaces coated with the indicated proportion of MCC:I-E^{k} diluted into Hb:I-E^{k}. **(I-L)** Data correspond to bar graphs in Figure 4I-L. For all data but H, N = number of cells analyzed. For (**H**), dots equal mean +/- SEM for the $t_{1/2}$ values determined in multiple individual experiments. For CD4T^{mCh+}: N=16 (100%); N=4 (50%); N=3 (12.5%); N=1 (4%); N=6 (0%) individual experiments. For CD4T$^{\Delta bind.\ mCh+}$: N=17 (100%); N=4 (50%); N=3 (12.5%); N=1 (4%); N=6 (0%) individual experiments. Between 20-60 cells were analyzed per experiment.

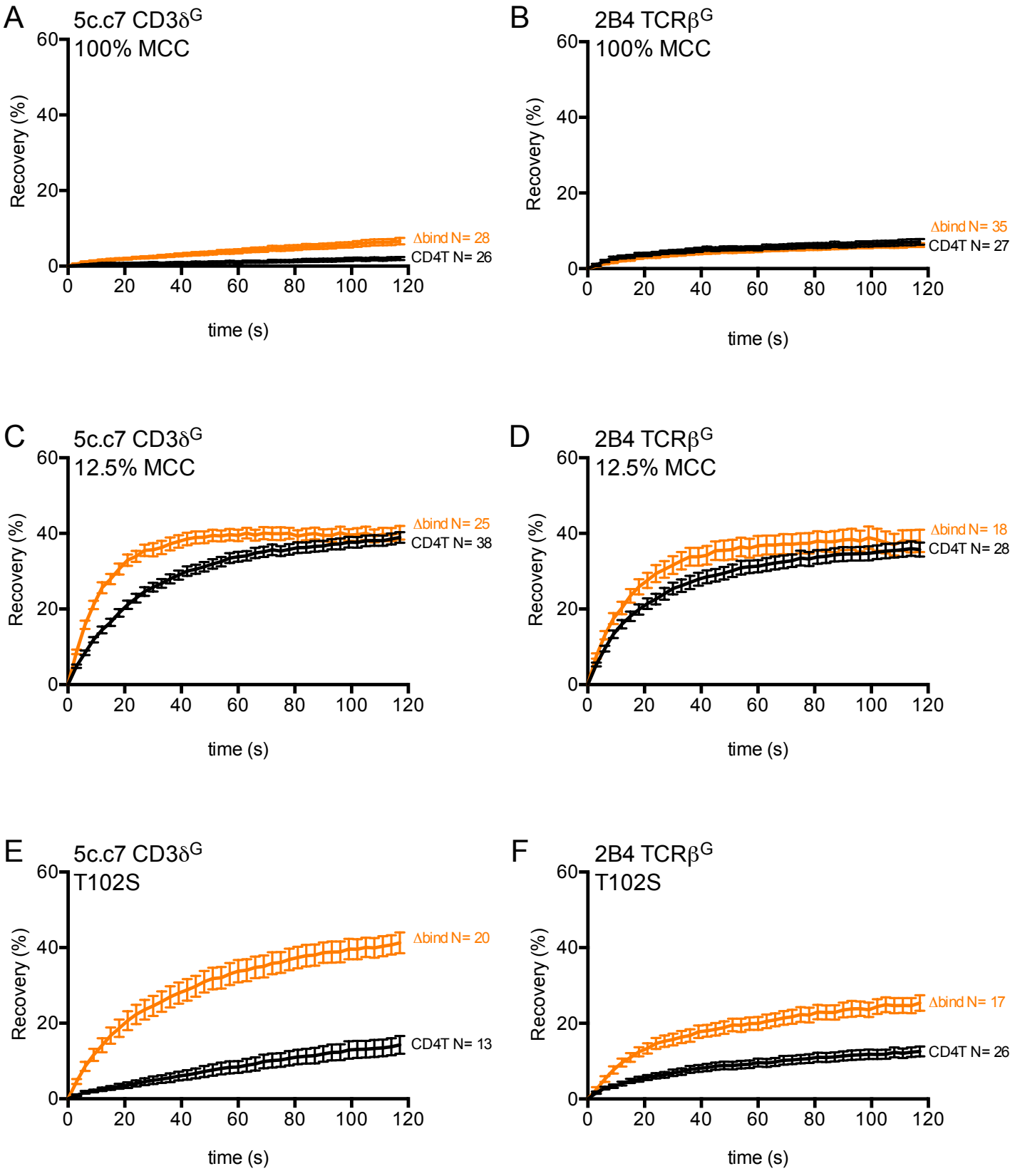
A
5c.c7 CD3δ^G
100% MCC
Recovery (%)
time (s)
Δbind N= 28
CD4T N= 26
B
2B4 TCRβ^G
100% MCC
Recovery (%)
time (s)
Δbind N= 35
CD4T N= 27
C
5c.c7 CD3δ^G
12.5% MCC
Recovery (%)
time (s)
Δbind N= 25
CD4T N= 38
D
2B4 TCRβ^G
12.5% MCC
Recovery (%)
time (s)
Δbind N= 18
CD4T N= 28
E
5c.c7 CD3δ^G
T102S
Recovery (%)
time (s)
Δbind N= 20
CD4T N= 13
F
2B4 TCRβ^G
T102S
Recovery (%)
time (s)
Δbind N= 17
CD4T N= 26

Figure S5

Figure S5. TCR-CD3 recovery, related to Figure 5.
M12 cells were transduced with genes encoding 5c.c7α, 5c.c7β, truncated CD3 subunits with CD3δT^{G} and CD4T^{mCh} or 2B4α, 2B4β^{G}, CD3T and CD4T^{mCh}. **(A-F)** TCR-CD3 recovery traces of M12 cells on immobile surfaces coated with 100% MCC:I-E^{k} (**A-B**), 12.5% MCC:I-E^{k} diluted into Hb:I-E^{k} (**C-D**), or T102S:I-E^{k} (**E-F**). N = number of cells analyzed.

A

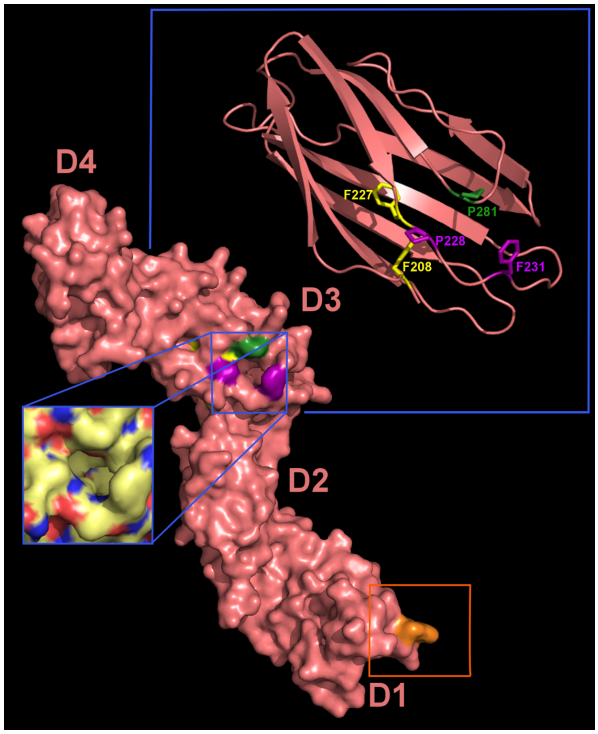

B

Mouse:	FPLNF	Mouse:	GKGVLIR
Rat:	FPLNL	Rat:	NK--LLI
Human:	FPLAF	Human:	GS--FLT
Monkey:	FPLAF	Monkey:	GS--FVT
Cat:	FPLNF	Cat:	HPSLCLT
Dog:	FPLSF	Dog:	GSFWTV-
Goat:	FPLTF	Goat:	NS--FLH
CD4 D3	aa227-231	CD4 D1	aa67-73
WT:	FPLNF	WT:	GKGVLIR
P228E+F231E:	FELNE	Δbind:	GDGDSDS

Mouse:	ETLPL
Human:	KKLPL
Rat:	ETLPL
Monkey:	KKLPF
Cat:	DSLPL
Dog:	ESLPL
Goat:	ERLPL
CD4 D3	aa278-282
WT:	ETLPL
P281E:	ETLEL

C

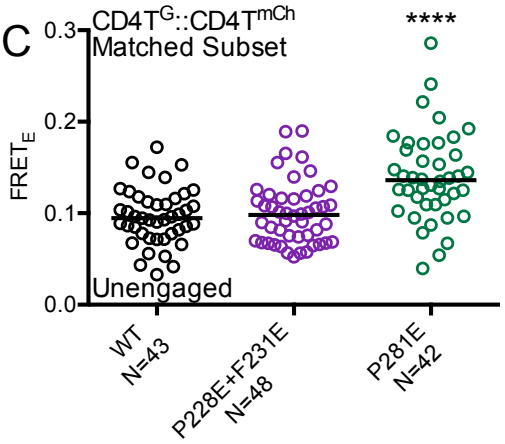

D

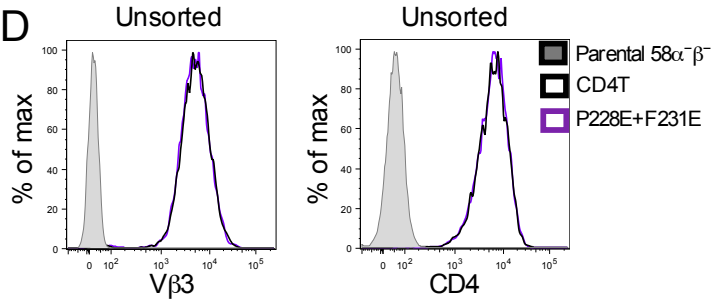

E

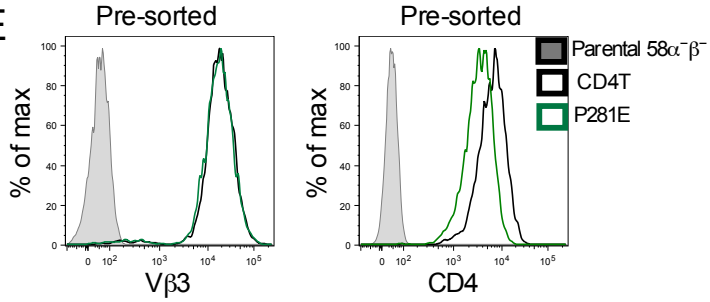

F

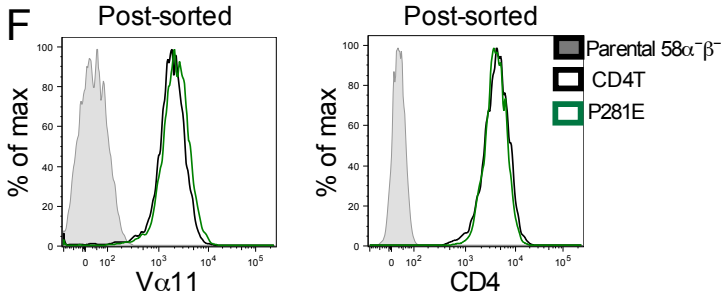

G

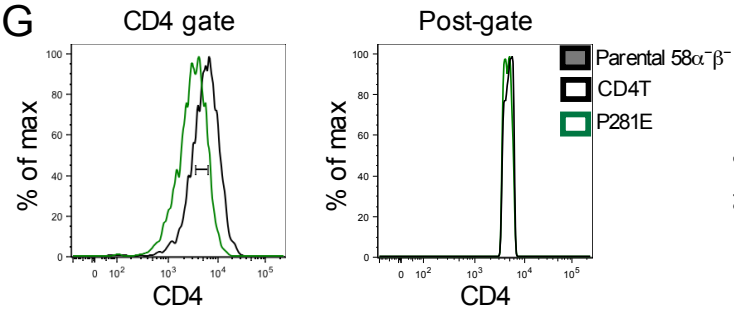

H

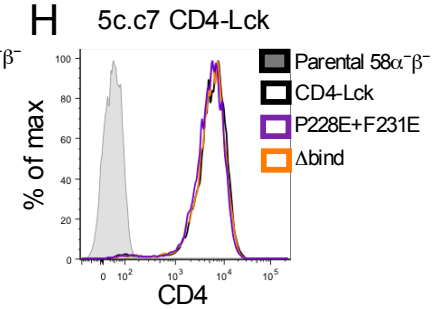

Figure S6

Figure S6. Residues mutated in the CD4 D1 and D3 domains, related to Figure 6.
(**A**) A surface rendered structure of hCD4 (PDB: 1WIO) is shown in Salmon with the D1, D2, D3, and D4 domains labeled. The orange box around residues in the C-terminal D1 domain highlight the MHCII contact site identified in previous structural analysis (Wang et al., 2001; Yin et al., 2012). Orange residues highlight those mutated for the Δbind mutant used in this study (Parrish et al., 2015). The D3 domain solvent exposed residues P228 (purple), F231 (purple), and P281 residues (green) mutated in this study are shown along with the hydrophobic core residues F208 and F227 (yellow) that were previously studied (Vignali and Vignali, 1999). The D3 domain is also shown as a cartoon structure to better highlight these colored residues (upper inset). The nonpolar patch created by P228, F231, and P281 is shown (lower inset) colored by atoms (carbon = yellow, hydrogen = grey, oxygen = red, nitrogen = blue). Images were generated with the PyMOL Molecular Graphics System, Version 1.8 Schrödinger, LLC.
(**B**) Sequence alignment of the CD4 D3 domain residues targeted for mutagenesis. The mutants generated for this study are shown color-coded as in the structure.
(**C**) Donor recovery after acceptor photobleaching of WT or mutant $CD4^{mCh}$::$CD4^{GFP}$ on glass coverslips (unengaged). Data are representative of three independent experiments and were assessed for normality using a D'Agostino and Pearson omnibus normality test followed by a one-way analysis of variance (ANOVA) and Dunnet's multiple comparison test (*$p<0.05$). N = number of cells analyzed.
(**D**) Surface expression of TCR (Vβ3) and CD4 on $5c.c7^{+}58\alpha^{-}\beta^{-}$ cells expressing wild-type CD4 or the P228E+F231E mutations.
(**E**) The P281E mutation reduces CD4 surface expression. (**F**) Sorting for matched expression.
(**G**) Representative example of matched gating used for quantification of CD69 upregulation and TCR downregulation for non-sorted cell lines.
(**H**) Surface expression of CD4 on $5c.c7^{+}58\alpha^{-}\beta^{-}$ cells expressing wild-type CD4-Lck or the P228E+F231E and Δbind mutations.

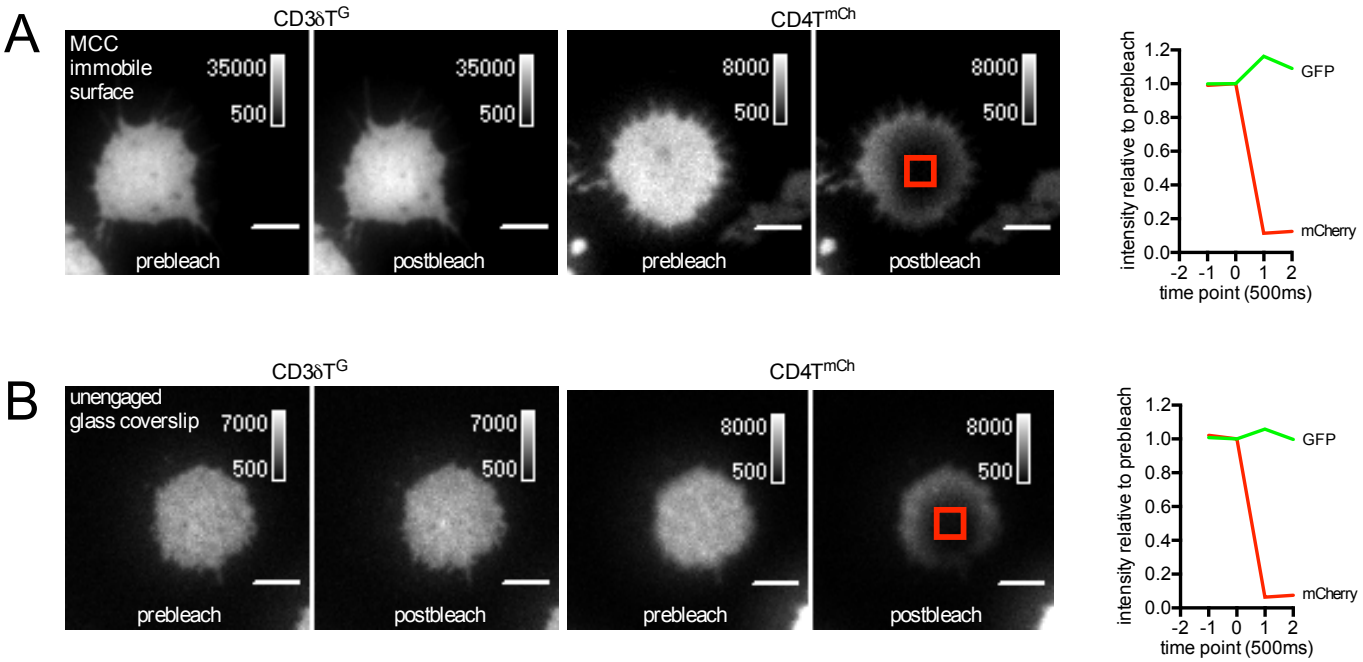
A
CD3δT^G
CD4T^mCh
MCC
immobile
surface
35000
500
8000
prebleach
postbleach
intensity relative to prebleach
GFP
mCherry
time point (500ms)
B
unengaged
glass coverslip
7000

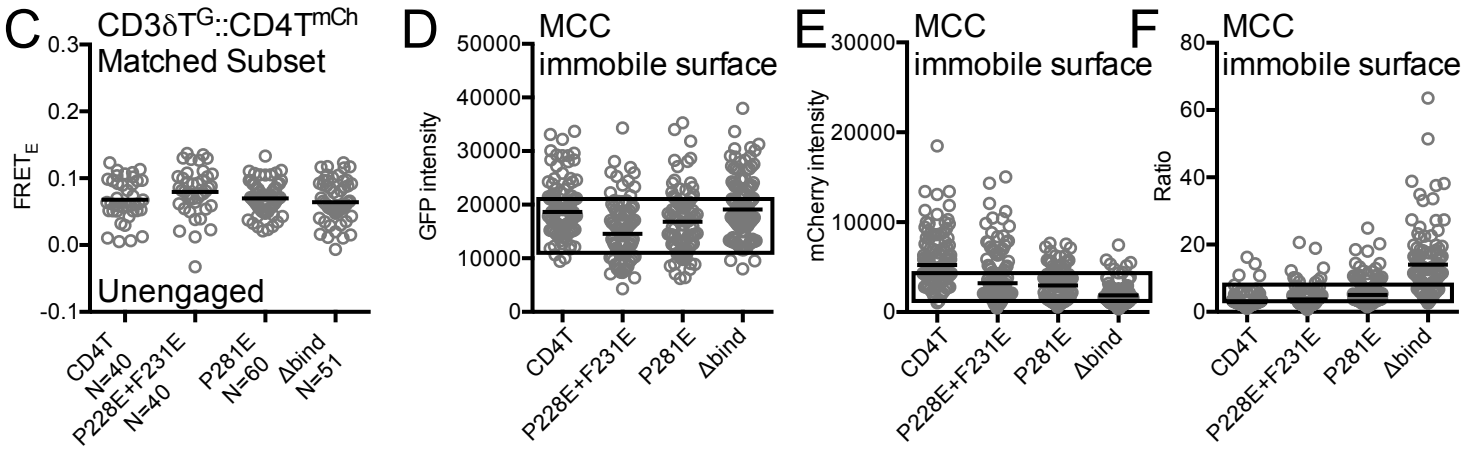
C
CD3δT^G::CD4T^mCh
Matched Subset
FRET_E
Unengaged
CD4T N=40
P228E+F231E N=40
P281E N=60
Δbind N=51
D
MCC
immobile surface
GFP intensity
E
mCherry intensity
F
Ratio

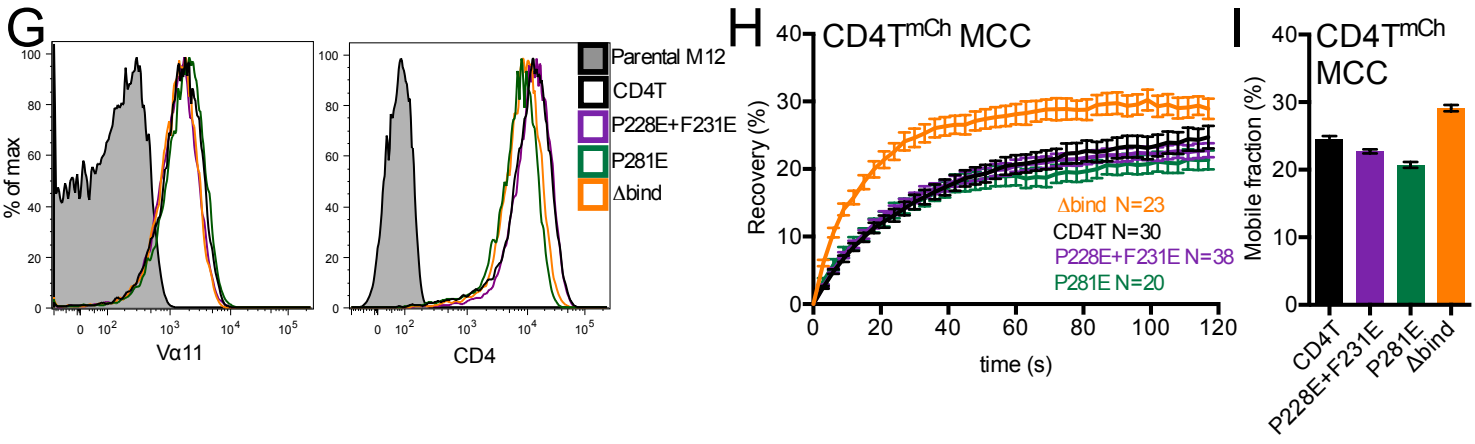
G
% of max
Vα11
CD4
Parental M12
CD4T
P228E+F231E
P281E
Δbind
H
CD4T^mCh MCC
Recovery (%)
time (s)
Δbind N=23
CD4T N=30
P228E+F231E N=38
P281E N=20
I
Mobile fraction (%)

Figure S7

Figure S7. Impact of D3 domain mutants on macrocomplex assembly, related to Figure 7.
(**A-B**) Donor recovery after acceptor photobleaching. Example images and traces are shown for 5c.c7^{+} M12 cells expressing CD3T subunits and CD4T adhered to (**A**) MCC:I-E^{k} coated surfaces, or (**B**) glass coverslips. Background subtracted images show mEGFP (CD3δT^{G}) and mCherry (CD4T^{mCh}) before and after photobleaching. The red box indicates region of interest (ROI). Scale bars represent 5μm and look up tables indicate intensity units for the indicated channels. Traces to the right show mEGFP (green) and mCherry (red) intensities relative to prebleach. Images were acquired at 500ms intervals.
(**C**) Donor recovery after acceptor photobleaching of WT CD4 and mutants on glass coverslips (unengaged). Data are representative of two experiments and were assessed for normality using a D'Agostino and Pearson omnibus normality test followed by a one-way analysis of variance (ANOVA) and Dunnet's multiple comparison test.
(**D-F**) Subset analysis for FRET. Analyzed populations had photobleaching <12.5% of the mCherry prebleach intensity and were matched for (**D**) mEGFP intensity (postbleach), (**E**) mCherry intensity (prebleach) and (**F**) mEGFP/mCherry ratio in TIRF.
(**G**) TCR (Vα11) and CD4 (GK1.5) surface expression on 5c.c7^{+} M12 cells.
(**H-I**) mCherry recovery and mobile fraction of the indicated CD4T mutants adhered to MCC:I-E^{k} coated surfaces. Data are presented as in Figure 3D-E. N = number of cells analyzed.